Tunnel Electrode I. Electron Transfer Process at Highly Doped SnO_2 Electrode with Ce^{4+} in High Overvoltage Region

Kenkichiro KOBAYASHI,* Yoshihiro AIKAWA, and Mitsunori SUKIGARA
Institute of Industrial Science, The University of Tokyo,
7-22-1 Roppongi, Minato-ku, Tokyo 106
(Received February 24, 1982)

Electron transfer theory at tunnel semiconductor electrode was derived from the double adiabatic perturbation theory. The cathodic current of Ce^{4+} with very positive redox potential was measured at highly doped SnO_2 electrode. The rearrangement energy of 0.65 eV for Ce^{4+} was estimated from the relationship of transfer coefficient *vs.* electrode potential. Large electron transfer rate in the high overvoltage region can be explained in terms of the contribution of excited vibrational states in the first coordination sphere into electron transfer.

The effect of electrode potential on the characteristics of an usual semiconductor electrode is such that the electrode potential cannot modify the energy of electrons and holes at the surface, but can change the surface density of electrons and holes through the band bending. When the carrier density of a semiconductor is very large, the thickness of the space charge layer is so small that electrons or holes can move through the depletion layer by tunneling. If such a highly doped semiconductor is used as an electrode, the electron transfer by tunneling through the space charge layer and the Helmholtz layer may occur in a certain potential range.[1-3] Thus, such a electrode may be called "tunnel semiconductor electrode." The electrochemical characteristic of a tunnel electrode is that the energy of a transferring electron or hole can be easily varied by the electrode potential.

For the rate of electron transfer reactions, Marcus[4] predicted that, in the so called normal region where the energy change of a reaction, $|\Delta E|$, is smaller than the rearrangement energy λ_s, the reaction rate should increase with $|\Delta E|$, while in the abnormal region where $|\Delta E|>\lambda_s$, the reaction rate should decrease with $|\Delta E|$. Rhem and Weller,[5,6] however, reported that such a decrease in the reaction rate was not observed in the abnormal region. Although their experimental results are significant, the electron transfer rate in the abnormal region could not be quantitatively discussed because of the diffusion limit of their reactions. The electrochemical electron transfer rate in the abnormal region has not been studied with metal electrode, because the electrons are distributed over a wide energy range in a metal. On the other hand, a tunnel electrode has an electron distribution in a definite and narrow energy range, so that the observed current directly reflects on the transition probability of electron with the semiconductor Fermi level. Therefore, the tunnel electrode is especially a useful tool for the measurement of electron transfer rate in the abnormal region.[7] The tunnel electrode has another advantage that the tunneling probability is usually not so high that the current may not be limited by diffusion even in a high overvoltage region.

In the present work, a theory for the cathodic tunnel current is derived and, by measuring the cathodic tunnel current at a highly doped tin oxide electrode, the electron transfer mechanism of Ce^{4+} at high overvoltage is discussed.

Theoretical

The cathodic and anodic current density at n-type tunnel electrode are respectively given by[8]

$$i_c = -ed\Omega C_{ox}\int W_c(E)\rho_{sc}(E)f(E)\mathrm{d}E, \quad (1)$$

and

$$i_a = ed\Omega C_{red}\int W_a(E)\rho_{sc}(E)[1-f(E)]\mathrm{d}E, \quad (2)$$

where W_c and W_a are respectively the transition probability for cathodic and anodic processes, $\rho_{sc}(E)$ is the state density in the semiconductor bulk, $f(E)$ is the Fermi distribution function, C_{ox} and C_{red} are respectively the concentration of the oxidant and that of reductant, d is the distance from the electrode surface, at which the transition probability is the greatest, E denotes the energy of transferring electron, e is the elementary charge, and Ω is the volume of the electrode.

The transition probability, $W_c(E)$, can be derived from the adiabatic perturbation theory considering the vibration in the first coordination sphere and given by[9-11]

$$W_c(E) = \frac{2\pi}{\hbar}|\langle\psi_f|V_{int}|\psi_i\rangle|^2\rho_{red}(E), \quad (3)$$

where ρ_{red} corresponds to the state density which is given by,[9-11]

$$\rho_{red}(E) = \left(\frac{1}{4\pi kT\lambda_s}\right)^{1/2} \times \sum_{m=-\infty}^{\infty}\exp\left[-(E-E^\circ_{redox}-\lambda_s-m\hbar\omega_c)^2/4kT\lambda_s\right] \times \exp\left[-Z_c\cosh\left(\frac{\hbar\omega_c}{2kT}\right)+\frac{m\hbar\omega_c}{kT}\right]I_m(Z_c), \quad (4)$$

where $Z_c=(1/2)\Delta_c^2\ \mathrm{cosec}\ (\hbar\omega_c/2kT)$, $I_m(Z_c)=(Z_c/2)_m\times\sum_{k=0}^{\infty}(Z_c/2)^{2k}/[k!\times(m+k)!]$, ψ_f denotes the unperturbed electronic wave function for the final state where an electron is located at an ion in solvent, ψ_i denotes the unperturbed electronic wave function for the initial state where an electron is located in semiconductor, V_{int} is the electronic interaction causing electron transfer, $\hbar\omega_c$ is the vibrational energy of the first coordination sphere, λ_s represents the rearrangement energy of solvent, E°_{redox} is the electronic energy corresponding to the standard redox potential, V°, and Δ_c is the difference between the equilibrium normal

coordinates of the vibration in the first coordination sphere in the initial state and those in the final state.

Similarly, the transition probability for anodic current, $W_a(E)$, is given by[9-11]

$$W_a(E) = \frac{2\pi}{\hbar}|\langle\phi_f|V_{int}|\phi_i\rangle|^2\rho_{ox}(E), \quad (5)$$

where

$$\rho_{ox}(E) = \left(\frac{1}{4\pi kT\lambda_s}\right)^{1/2} \times \sum_{m=-\infty}^{\infty} \exp\left[-(E^\circ_{redox}-E-\lambda_s-m\hbar\omega_c)^2/4kT\lambda_s\right] \times \exp\left[-Z_c\cosh\left(\frac{\hbar\omega_c}{2kT}\right)+\frac{m\hbar\omega_c}{2kT}\right]I_m(Z_c). \quad (6)$$

The square of the matrix element $|\langle\phi_f|V_{int}|\phi_i\rangle|^2$ can be rewritten as[12]

$$|\langle\phi_i|V_{int}|\phi_f\rangle|^2 = Pr|\langle\phi_f|V'_{int}|\phi'_i\rangle|^2, \quad (7)$$

where Pr represents the tunneling probability through the space charge layer, and $\langle\phi_f|V'_{int}|\phi'_i\rangle$ denotes approximately the matrix element causing electron transfer through the Helmholtz layer.

The tunneling probability Pr was calculated with the WKB approximation, assuming the Schottky type barrier and the two band model[13] for the energy-complex momentum relationship in the forbidden gap. In the case of a semiconductor with wide gap energy, the probability for the direct tunneling through the space charge layer is given by[14]

$$Pr = C_1\exp\left[-\frac{2}{\hbar}\left(\frac{m^*\varepsilon_{sc}}{n}\right)^{1/2}\phi_{sc}\right], \quad (8)$$

where m^* is the effective mass, ε_{sc} is the permittivity of semiconductor, ϕ_{sc} denotes the band bending, n is the electron density in the semiconductor bulk,[15] and C_1 is slowly varying function of the band bending, *etc.* With the decrease of carrier density, the probability for the direct tunneling decrease quickly, and thus the indirect tunneling *via* trapping states in the space charge layer becomes important. If the indirect tunneling occurs *via* one trapping state, the tunneling probability for this process is given by[14]

$$Pr = C_2\exp\left[-\frac{1}{\hbar}\left(\frac{m^*\varepsilon_{sc}}{n}\right)^{1/2}\phi_{sc}\right], \quad (9)$$

where C_2 is slowly varying function of the band bending, *etc.*

Figure 1 shows the energy relationship at a semiconductor/electrolyte interface. We consider then a highly doped SnO_2 electrode as an example. In the case of parabolic model for $\rho_{sc}(E)$, the Fermi level of SnO_2 with $n=10^{19}$ cm^{-3}, $m^*=0.22\,m$ and $\varepsilon_{sc}=10\,\varepsilon_0$ is located at 0.07 eV above the bottom of conduction band, and electrons are distributed in a narrow energy range near the Fermi level. Thus, if the tunneling through the space charge layer is dominant, $\rho_{sc}(E)f(E)$ can be approximated by

$$\rho_{sc}(E)f(E) = n\delta(E+eV), \quad (10)$$

where n is the carrier density, V is the electrode potential, and δ is the Dirac δ function. The validity of this approximation will be discussed later.

Substituting Eq. 10 and the relation of $E_{redox}=-eV^\circ$ into Eq. 1, the cathodic current density is written as

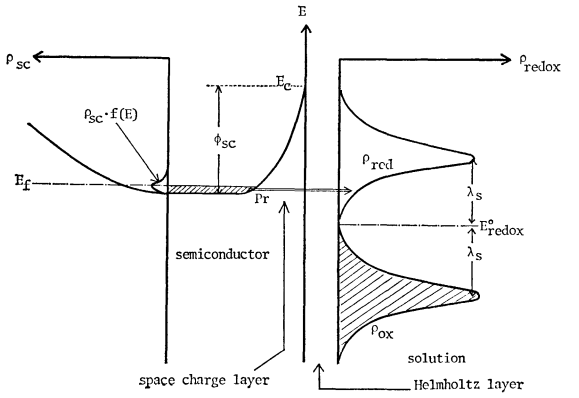

Fig. 1. Schematic representation of electron transfer under more positive potential than flat band potential at a highly doped semiconductor/electrolyte interface.

$$i_c = -edn\Omega C_{ox} \times \frac{2\pi}{\hbar}|\langle\phi_f|V'_{int}|\phi'_i\rangle|^2 \times Pr \times \rho_{red}(-eV), \quad (11)$$

where

$$\rho_{red}(-eV) = \left(\frac{1}{4\pi KT\lambda_s}\right)^{1/2} \times \sum_{m=-\infty}^{\infty} \exp\left[-(-eV+eV^\circ-\lambda_s-m\hbar\omega_c)^2/4kT\lambda_s\right] \times \exp\left[-Z_c\cosh\left(\hbar\omega_c/2kT\right)+m\hbar\omega_c/2kT\right]I_m(Z_c). \quad (12)$$

Equation 11 indicates that the magnitude of tunnel current directly reflects the transition probability at semiconductor Fermi level which can be defined by the electrode potential. On the other hand, the integral in Eq. 2 cannot be removed by the use of Eq. 10; the anodic current at an n-type semiconductor tunnel electrode contains all the electron transfer processes at various energy levels. Then, it is difficult to determine the transition probability from the experimental anodic tunnel current. In the present work, only the cathodic tunnel current at tunnel n-type semiconductor electrode is discussed.

The band bending, ϕ_{sc}, at more positive potential than the flat band potential is a function of the electrode potential, V, as follows:[3]

$$\phi_{sc}^{1/2} = \frac{1}{2}[-K+(K^2+4V-4V_{fb})^{1/2}]. \quad (13)$$

Here,

$$K = \frac{d_H}{\varepsilon_H}(2\varepsilon_{sc}nq)^{1/2}, \quad (14)$$

where V_{fb} is the flat band potential, d_H is the thickness of the Helmholtz layer, and ε_H is the permittivity of the Helmholtz layer. Then, the transfer coefficient, α, is given by

$$\alpha \equiv -\frac{kT}{e}\frac{\partial\ln(-i_c)}{\partial V} = \alpha_T + \alpha_\rho, \quad (15)$$

where $\alpha_T\equiv(-kT/e)(\partial\ln Pr/\partial V)$ is the transfer coefficient due to the tunneling through the space charge layer and is given by

$$\alpha_T \equiv \frac{kT}{e}\frac{2}{\hbar}\left(\frac{m^*\varepsilon_{sc}}{n}\right)^{1/2}\{1-K(K^2+4V-4V_{fb})^{-1/2}\}, \quad (16)$$

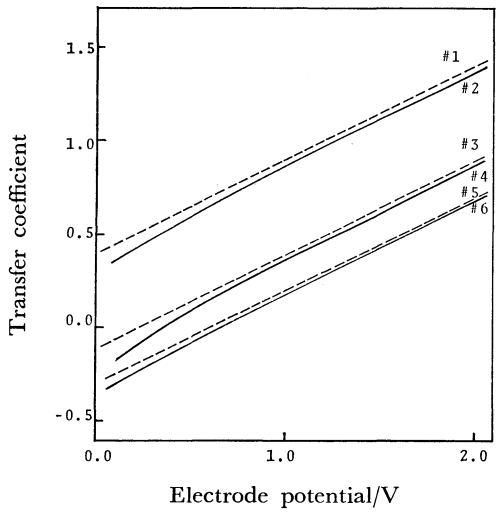

Fig. 2. Relationship between transfer coefficient and electrode potential in high temperature limiting case (T=300 K, λ_s=0.6 eV, $\hbar\omega_c$=0.002 eV, Δ_c=20, λ_c=0.4 eV, $V°$=2.0 V, V_{fb}=0.0 V, $\varepsilon_{sc}=10\varepsilon_o$, $m^*=0.2\,m$, $\varepsilon_H=6\varepsilon_o$, d_H=0.3 nm). #1 and #2: $n=5\times10^{18}$ cm^{-3}, #3 and #4: $n=2.7\times10^{19}$ cm^{-3}, #5 and #6: $n=1.0\times10^{20}$ cm^{-3}. Solid lines are α-V curves considering potential drop across the Helmholtz layer, ϕ_H. Broken lines are α-V curves neglecting ϕ_H.

for the direct tunneling, and

$$\alpha_T \equiv \frac{kT}{e}\frac{1}{\hbar}\left(\frac{m^*\varepsilon_{sc}}{n}\right)^{1/2}\{1-K(K^2+4V-4V_{fb})^{-1/2}\}, \quad (17)$$

for the indirect tunneling with one trapping state, and $\alpha_\rho \equiv (-KT/e)(\partial \ln \rho_{red}/\partial V)$ is the transfer coefficient depending on the state density for acceptor state.

In case of $\hbar\omega_c \ll kT$, the transfer coefficient α_ρ is written as[16]

$$\alpha_\rho = \frac{eV-eV°+\lambda_s+(1/2)\hbar\omega_c\Delta_c^2}{2(\lambda_s+(1/2)\hbar\omega_c\Delta_c^2)}. \quad (18)$$

In case of $\hbar\omega_c \gg kT$, the transfer coefficient α_ρ in the normal region, *i.e.* $V>V°-\lambda_s/e$, is given by

$$\alpha_\rho = \frac{eV-eV°+\lambda_s}{2\lambda_s}, \quad (19)$$

while in the abnormal region, *i.e.* $V<V°-\lambda_s/e$,

$$\alpha_\rho = -\frac{kT}{e}\frac{\partial \ln}{\partial V}\left\{\sum_{m=0}^{\infty}\exp\left[-\frac{(-eV+eV°-\lambda_s-m\hbar\omega_c)^2}{4kT\lambda_s}\right]\times\frac{1}{m!}\left(\frac{\Delta_c^2}{2}\right)^m\right\}, \quad (20)$$

and it oscillates with the period, $V_p=\hbar\omega_c/e$, when the electrode potential is swept. In the intermediate case, *i.e.* $\hbar\omega_c \approx kT$,[9]

$$\alpha_\rho = \frac{e(V-V°)+\lambda_s}{2\lambda_s}+\frac{kT}{\lambda_s}\frac{\Delta_c^2}{2}\frac{\hbar\omega_c}{2kT}\,\mathrm{cosech}\left(\frac{\hbar\omega_c}{2kT}\right)\times\sinh\left[\frac{\hbar\omega_c(-eV+eV°)}{2kT\lambda_s}\right] \quad (21)$$

Broken lines in Figs. 2, 3, and 4 show the α-V curves neglecting the potential drop across the Helmholtz layer for $\hbar\omega_c \ll KT$, $\hbar\omega_c \gg KT$, and $\hbar\omega_c \approx KT$, respectively. In the high temperature limiting case, the slope of α-V curves is $(2\lambda_s+\hbar\omega_c\Delta_c^2)^{-1}$, and

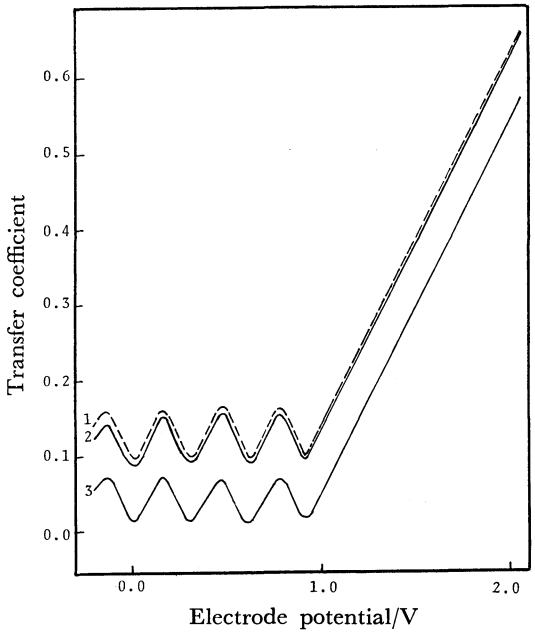

Fig. 3. Relationship between transfer coefficient and electrode potential in low temperature limiting case (T=30 K, $\hbar\omega_c$=0.3 eV, λ_s=1.0 eV, $\varepsilon_H=6\varepsilon_o$, d_H=0.3 nm, $\Delta_c=2^{1/2}$, $V°$=2.0 V). Curves of 1 and 2 are α-V curves at semiconductor with V_{fb}=0.0 V, m^*=0.1 m, $\varepsilon_{sc}=5\varepsilon_o$, and $n=10^{19}$ cm^{-3} in case of neglecting ϕ_H and that in case of considering ϕ_H, respectively. Curve 3 corresponds to α_T=0.

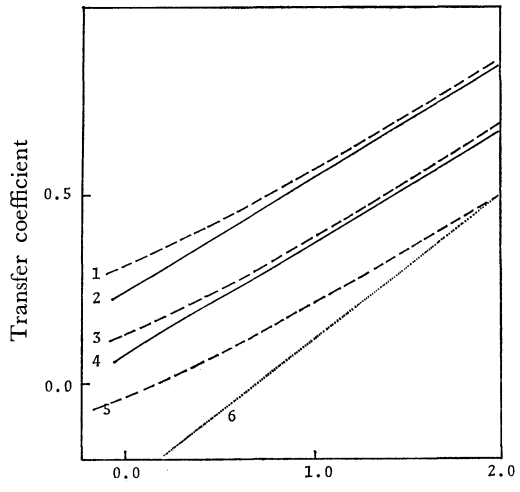

Fig. 4. Relationship between transfer coefficient and electrode potential in intermediate case (T=300 K, $\hbar\omega_c$=0.06 eV, λ_s=0.6 eV, m^*=0.2 m, $\varepsilon_{sc}=10\varepsilon_o$, Δ_c=2, V_{fb}=0.0 V, $V°$=2.0 V).
1 and 2: $n=2.7\times10^{19}$ cm^{-3}, 3 and 4: $n=1.0\times10^{20}$ cm^{-3}, 5: α_T=0.0. Dotted line is α-V curve neglecting ϕ_H and change of Δ_c (Δ_c=0). Broken lines are α-V curves neglecting ϕ_H. Solid lines are α-V curves considering ϕ_H.

there is not difference in α-V curve between the normal and abnormal regions. In the low temperature limiting case, electron transfer is accompanied by the nuclear tunneling in the first coordination sphere. Then, the slope of α-V curves in the normal region

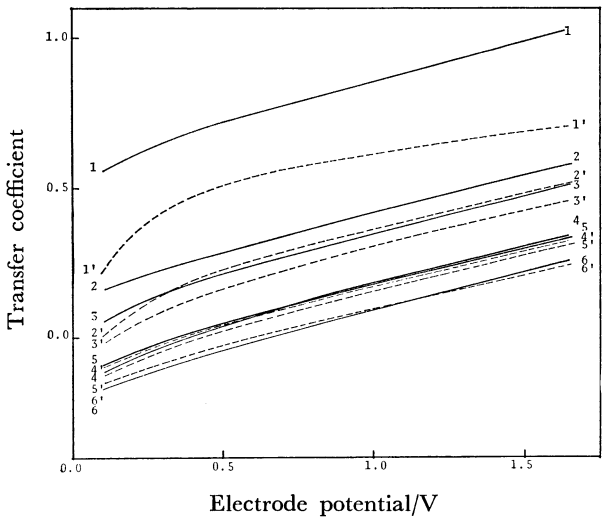

Fig. 5. Relationship between transfer coefficient and electrode potential ($T=300$ K, $\lambda_s=1.0$ eV, $\lambda_c=1.0$ eV, $\lambda_c=1.0$ eV, $\hbar\omega_c=0.002$ eV, $\Delta_c=22.3$, $V^\circ=3.0$ V, $V_{fb}=0.0$ V, $\varepsilon_{sc}=10\varepsilon_o$, $m^*=0.2\ m$). Solid lines are α-V curves calculated with Eq. 10. Broken lines are α-V curves calculated without Eq. 10. 1,1′,3,3′,5,5′: direct tunneling; 2,2′,4,4′,6,6′: indirect tunneling. 1,1′,2,2′: $n=5\times10^{18}$ cm^{-3}; 3,3′,4,4′: $n=2.7\times10^{19}$ cm^{-3}; 5,5′,6,6′: $n=1.0\times10^{20}$ cm^{-3}.

is $(2\lambda_s)^{-1}$ because both the initial vibrational state and the final state are the ground states, while α-V curves in the abnormal region oscillate with the period, $\hbar\omega_c$, because of the significant contribution of an excited vibrational state in the final state. In the intermediate case, the nuclear tunneling in the first coordination sphere occurs to some extent, and the slope of α-V curves in small overvoltage region is approximately $(2\lambda_s)^{-1}$.

The solid lines in Figs. 2, 3, and 4 show the α-V curves considering the potential drop across the Helmholtz layer. In determing the rearrangement energy of solvent from the α-V curve, the effect of the potential drop across the Helmholtz layer on the transfer coefficient is not significant, except for the region near the flat band potential.

Here we consider the validity of the approximation in Eq. 10. Figure 5 shows the α-V curves corresponding to the high temperature limiting case. The broken lines in Fig. 5 are α-V curves calculated numerically without using the approximation given in Eq. 10. The α-V curves calculated with Eq. 10 are also shown by solid lines in Fig. 5. The good agreement between the solid lines of 3 to 6 and the broken lines of 3′ to 6′ indicates that the approximation of Eq. 10 is reasonable under the condition, $n\geqq2.7\times10^{19}$ cm^{-3}, $m^*=0.2\ m$, and $\varepsilon_{sc}=10\ \varepsilon_o$, at room temperature. However, the broken line (1′) deviates from the solid line (1). This deviation is interpreted in terms of a considerable contribution of the thermal excitation in the total current. This result means that the approximation given by Eq. 10 is no longer applicable when the carrier concentration is less than 5×10^{18} cm^{-3} at room temperature.

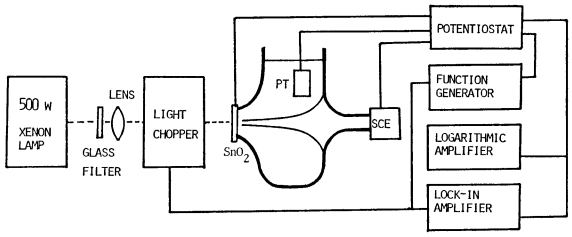

Fig. 6. Diagram of the experimental setup.

Experimental

Tin oxide coated glasses supplied from Matsuzaki Vacuum Co. and those from Asahi Glass Co. were made by the spray and vacuum evaporation methods, respectively. The former tin oxide layer has been doped with Sb and the latter has a high density O_2-vacancy. The surface area of each electrode was about 0.8 cm^2. The thickness of the SnO_2 layer was measured by a surface roughness meter. Ceric sulfate of commercially available reagent grade was used without further purification. The experimental setup is shown in Fig. 6. A saturated calomel electrode and a large area platinum disk electrode were used as the reference electrode and the counter electrode, respectively. In order to determine the flat band potential at various pH values, photocurrents by the band gap excitation were measured with a chopped light and a lock-in amplifier. Buffered solutions of pH 3, 5, and 7 were prepared with 0.2 M (1 M=1 mol dm^{-3}) citric acid and sodium dihydrogenphosphate. Differential capacitance measurements were made by modulating the electrode potential with a 10 mV sine wave of 120—1000 Hz and by balancing the bridge. The transfer coefficient was obtained by using a logarithmic amplifier and a lock-in amplifier by modulating the electrode potential with a 0.2 mV square wave of 2 Hz. The steady state current was measured with the potential sweep rate of 2 mV/s.

Results and Discussion

The Measurement of the Properties of Tin Oxide Electrode. Figure 7 shows the relation between differential capacitance per unit area, C, and the electrode potential. As seen in Fig. 7, the plots of C^{-2} *vs.* applied potential show good linearity. This result indicates that the spatial distribution of the dopant in SnO_2 electrode is uniform, and that the depletion layer is formed under the anodic polarization. A frequency dependence in the capacitance was observed as shown in Fig. 7, but this may be interpreted in terms of the CR dispersion at the semiconductor/electrolyte interface[1] and the structural irregularity of the electrode surface.[17] The slopes of the plots in Fig. 7 should be proportional to N_D^{-1}, but the accurate carrier density could not be obtained from Fig. 7 without the knowledge of the surface factor.

The carrier density was determined directly by the Hall effect measurement. The carrier density of the SnO_2 electrodes thus obtained was in the range from 2.7×10^{19} to 3×10^{20} cm^{-3}. The large carrier density shows that the distribution of the carrier of those electrodes is degenerate. The surface factor was determined by comparing the carrier density obtained from the Hall effect with that from the slope of Mott-Schottky plot in Fig. 7.

TABLE 1. PROPERTIES OF TUNNEL SnO_2 ELECTRODES

Electrode #	Thickness[a] Å	Apparent carrier[b] concentration cm^{-3}	Carrier[c] concentration n cm^{-3}	Surface factor	Flat band[d] potential V_{fb} *vs.* SCE V
1	1450	4.5×10^{21}	3.1×10^{20}	3.8	0.20
2	3000	3.7×10^{22}	1.0×10^{20}	19.2	0.22
3	400	1.0×10^{21}	2.7×10^{19}	6.0	0.24

a) Thickness of the SnO_2 layers measured by Dr. R. Kimura of the Institute of Molecular Science in Japan. b) Values obtained from Mott-Schottky plot at 120 Hz. c) Values obtained from Hall effect. d) Values obtained at pH=0.3.

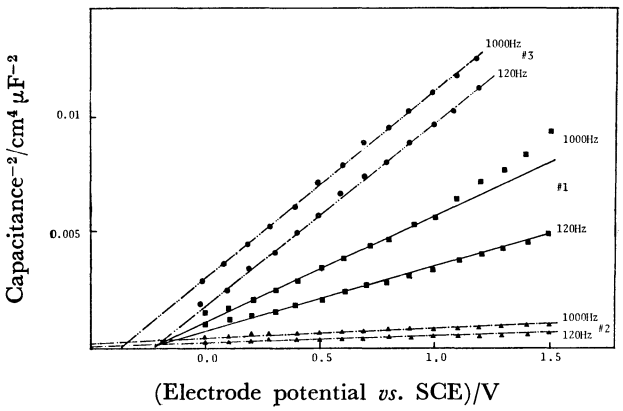

Fig. 7. Mott-Schottky plots for SnO_2 electrodes in a 0.25 M H_2SO_4.

The flat band potential, V_{fb}, of the SnO_2 electrode was determined from the onset potential of the anodic photocurrent[18] corresponding to O_2 evolution. The onset potential thus obtained agrees with the literature value.[19]

In Table 1 are listed the thickness of the tin oxide layer, the apparent carrier density from the slope of Mott-Schottky plot, the carrier density by the Hall effect, the surface factor and the flat band potential. The thickness of the electrode #3 is rather thin but is thicker than that of the depletion layer, *e.g.* 64 Å at 1.2 V *vs.* SCE. Table 1 also shows that the flat band potential shifts more negative with the increase of the carrier density, *i.e.* the Fermi level moves upper with the carrier density. The Fermi energy calculated by the parabolic model with $m^*=0.22m$[20] lies above the bottom of the conduction band, E_c: for the electrode #1; $E_F=E_c+0.66$ eV, #2; $E_c+0.39$ eV, and #3; $E_c+0.16$ eV. The difference among the above mentioned Fermi levels of these electrodes is significantly larger than the difference among the flat band potentials shown in Table 1. The discrepancy between the Fermi level thus calculated and the measured one has been often observed in the study of the tunnel diode,[21] and it was interpreted in terms of impurity band model.[22] Thus, the impurity band is formed in the SnO_2 electrode in this work. When the donor is O_2-vacancy or Sb, the relation between the donor density N_D and the donor ionization energy E_D for SnO_2 crystal has been given as[20]

$$E_D = 0.15 - 8.7\times10^{-8}N_D^{1/3} \quad [\text{eV}] \qquad (22)$$

The above relation means that the donor ionization energy approaches zero at a donor density of 5.5×10^{18} cm^{-3}. Since the carrier density of SnO_2 used in this work is larger than 10^{19} cm^{-3}, the shallow donor impurity band has been merged near the bottom of conduction band.

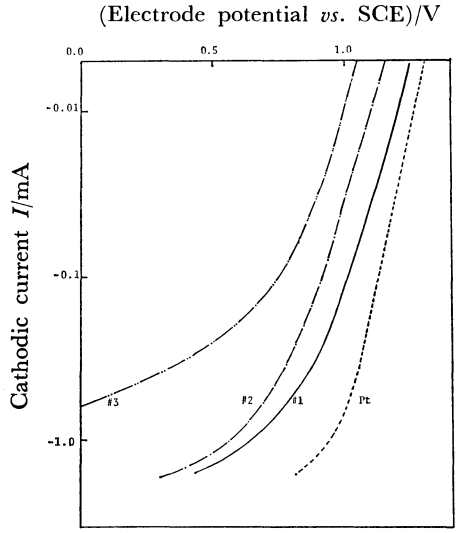

Fig. 8. Plots of cathodic tunnel current for the system of highly doped SnO_2–Ce^{4+} in a 0.25 M H_2SO_4 aqueous solution against electrode potential. #1: $n=3.1\times10^{20}$ cm^{-3}, #2: $n=1.0\times10^{20}$ cm^{-3}, #3: $n=2.7\times10^{19}$ cm^{-3}.

Cathodic Tunnel Current for Highly Doped SnO_2/Ce^{4+}. The steady state tunnel current was measured for Ce^{4+} which has very positive standard redox potential; $V^\circ(Ce^{4+/3+})=1.3$ V *vs.* SCE. In order to extend the potential region where the current is controlled by the electron transfer rate, a concentrated Ce^{4+} solution (0.5 M) was used. Figure 8 shows the curves of the cathodic current *vs.* electrode potential (*i-V*) for Ce^{4+} at SnO_2 electrodes in a 0.25 M H_2SO_4 aqueous solution. An *i-V* curve at a Pt electrode was also shown in Fig. 8 for comparison. As shown in Fig. 8 the magnitude of the current increases with the carrier density in SnO_2. The diffusion limited current is observed in the large current density region. In order to study the electron transfer mechanism in high overvoltage region, it is not suitable to use a too heavily doped semiconductor electrode because the current tends to become diffusion limited. However, a high carrier density is needed to ignore the thermal excitation current.

In Fig. 9 experimental values of the transfer coefficient, $\alpha(V)$, are plotted against electrode potential.

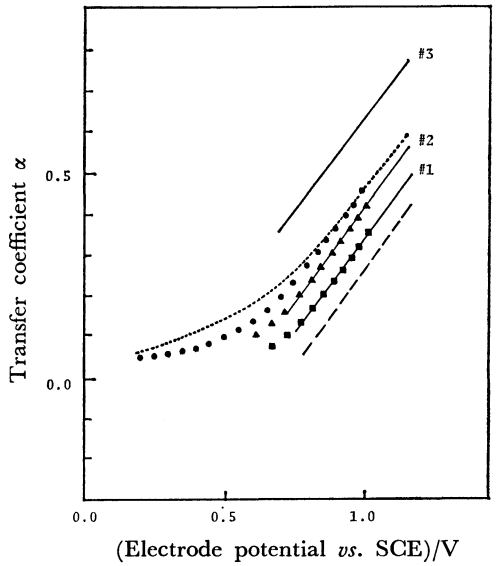

Fig. 9. Curves of transfer coefficient vs. electrode potential for 0.5 M Ce^{4+} at tunnel SnO_2 electrodes in a 0.25 M H_2SO_4 aqueous solution.
■,▲,●: Experimental values, ■ corresponds to #1, ▲ to #2 and ● to #3; solid lines: theoretical curves calculated with $m^*=0.21\ m$, $\lambda_s=0.65$ eV, and $V^\circ=1.3$ *vs.* SCE, broken line: solvent term, $1/2+e(V-V^\circ)/\lambda_s$, dotted line: theoretical curve for indirect tunneling at the electrode #3. #1: $n=3.1\times10^{20}$ cm^{-3}, #2: $n=1.0\times10^{20}$ cm^{-3}, #3: $n=2.7\times10^{19}$ cm^{-3}.

Since the amplitude of the modulation in obtaining α was such small value as 0.2 mV, higher order differential terms were negligible, and the pretty accurate values for $\partial \ln i/\partial V$ could be obtained. It seems from Fig. 8 that one can get constant values for the transfer coefficient in the potential range more positive than 1.0 V. However, in such region where the potential becomes near the equilibrium electrode potential, the contribution of the anodic process to the total current becomes so large that the effect of the anodic process on the transfer coefficient can not be neglected. Under such condition, α-V curve deviates from the theoretical one.

The plots in Fig. 9 show linearity in the potential region, $V>0.65$ V *vs.* SCE, and the slopes of these plots are almost same for three electrode. The plots shift with the carrier density of SnO_2 electrode. The slope of an α-V curve begins to change near $V=0.6$: the slope of an experimental α-V curve in the potential region, $V<0.6$, is much smaller. As mentioned in theoretical part, this α-V relationship implies that the electron transfer of Ce^{4+} corresponds to the intermediate case at room temperature. Thus, the rearrangement energy $\lambda_s=0.65$ eV for Ce^{4+} was determined from the slope of α-V in the small overvoltage region.

The rearrangement energy, λ_s, for Ce^{4+} or Ce^{3+} has been estimated by various methods. For instance, $\lambda_s=2.06$ eV[23] was determined from the electron transfer rate constant at a metal electrode by assuming the adiabatic electron transfer. Memming and Möller[19] estimated $\lambda_s=1.75$ eV by analyzing the anodic tunnel current at SnO_2. However, the Marcus theory[24] using the ion radius of Ce^{4+}, $R=3.77$ Å, has given $\lambda_s=0.5$ eV,[25] and the above values of λ_s seems too large. The overestimation of λ_s value determined from an electron transfer rate at a metal electrode is attributed to the break-down of the adiabatic electron transfer approximation: Ce^{4+} is so powerful oxidant that even a noble metal electrode is covered with a thin oxide layer in the potential region where the rates are measured. The electron transfer rate is mainly governed by the tunneling probability through the thin oxide film,[26] and the assumption of adiabatic electron transfer is not longer applied in this case. In addition, the nonadiabatic behaviour would be expected for the reduction of Ce^{4+} because the 4f orbitals involved in the reduction are strongly shielded by the 5s and 5p orbitals and the matrix element in Eq. 11 is expected to be very small.[27] In fact, the nonadiabatic electron transfer was found in the homogeneous redox reaction of $Eu^{2+/3+}$ in which $4f$ electron takes part in the electron transfer.[28]

The large λ_s-value reported by Memming and Möller[19] seems to be attributed to the complicated electron transfer mechanism of the anodic tunnel current at SnO_2 electrode: They calculated the anodic tunnel current by assuming the state density ρ_{ox} to be Gaussian function including the rearrangement energy, λ_s, as the parameter, and they determined the λ_s value by comparing the experimental tunnel i-V curve with the calculated one. In their calculation, however, they neglected the factors which might affect the tunnel i-V characteristics, that is, the indirect tunneling process, the excited vibrational states in the first coordination sphere, and the potential dependence of the state density in the conduction band, and the tunnel i-V characteristics were interpreted only in terms of the change in the rearrangement energy. Then, λ_s value thus estimated includes the rearrangement energy of the vibration in the first coordination sphere $(1/2)\hbar\omega_c\Delta_c^2$ as well as the contribution of the outersphere.

Three solid lines in Fig. 9 are the theoretical α-V curves, each of which is the sum of α_T in Eq. 16 and $\alpha_\rho=(eV-eV_0+0.65)/(2\times0.65)$. Two lines for the electrode #1 and #2 fit well will the experimental values, while for the electrode #3, the theoretical α-V curve does not fit with the experimental one. The small α_T for the electrode #3 indicates that the indirect tunneling process becomes significant in the tunneling through the space charge layer as expected in Eq. 17.

According to the values of standard redox potential for $Ce^{4+/3+}$, $V^\circ=1.3$ V *vs.* SCE and $\lambda_s=0.65$ eV for the cerium ion in an aqueous solution, the potential region more positive than 0.65 V *vs.* SCE corresponds to the normal region, and the region less than 0.65 V corresponds to the abnormal region. Linear relationship of α-V in the normal region leads to the Gaussian function for the acceptor state density, ρ_{red}. The dotted line in Fig. 9 was calculated with $\hbar\omega_c=400$ cm^{-1}, $\Delta_c=2.6$ by assuming the indirect tunneling (two step process). Those values of $\hbar\omega_c$ and Δ_c are typical ones[29] for the hydrated ions. Therefore, the small slope of α-V in the abnormal region is explained

by the contribution of the excited vibrational state in the first coordination sphere. If the λ_s-value is estimated formally from the potential dependence of the tunnel cathodic current in this abnormal region, one may obtain a unreasonably large value.[30]

Conclusion

The tunnel electrode appeared to be the very useful tool to study the electron transfer rate at high overvoltage. The λ_s-value of 0.65 eV for Ce^{4+} proved that this electron transfer process is nonadiabatic. Large electron transfer rate in the abnormal region could be explained by the significant contribution of the excited vibrational state in the first coordination sphere. The small tunnel transfer coefficient at SnO_2 #3 ($n = 2.7 \times 10^{19}$ cm^{-3}) implied that, in this case, the tunneling through the space charge layer involved the indirect tunneling *via* trapping states in the space charge layer.

The support of this research by Grant-in-Aid for Scientific Research, and Asahi Glass Foundation for Industrial Technology, is gratefully acknowledged.

References

1) D. Elliot, D. L. Zellmer, and H. A. Laitinen, *J. Electrochem. Soc.*, **117**, 1343 (1970).
2) B. Pettinger, H. R. Schöppel, and H. Gerischer, *Ber. Bunsenges. Phys. Chem.*, **78**, 450 (1974).
3) B. Pettinger, H. R. Schöppel, T. Yokoyama, and H. Gerischer, *Ber. Bunsenges. Phys. Chem.*, **78**, 1024 (1974).
4) R. A. Marcus, *J. Chem. Phys.*, **43**, 2654 (1965).
5) D. Rehm and A. Weller, *Israel J. Chem.*, **8**, 259 (1970).
6) H. Schonburg, H. Stark, and A. Weller, *Chem. Phys. Lett.*, **22**, 1 (1973).
7) K. Kobayashi, Y. Aikawa, and M. Sukigara, *J. Electroanal. Chem.*, **134**, 11 (1982).
8) V. G. Levich, "Advances in Electrochem. and Electrochem. Eng.," ed by P. Delahay and C. W. Tobias, Interscience New York (1966), Vol. 4, p. 249.
9) N. R. Kestner, J. Logan, and J. Jortner, *J. Phys. Chem.*, **78**, 2148 (1974).
10) J. Ulstrup and J. Jortner, *J. Chem. Phys.*, **63**, 4358 (1975).
11) V. G. Levich, "Physical Chemistry," ed by H. Eyring, D. Henderson, and W. Jost, Academic Press New York (1970), IXB 985.
12) W. A. Harrison, *Phys. Rev.*, **123**, 85 (1961).
13) W. Frang, "Handbuch der Physik, ed by S. Flugge, Springer Verlag, Berlin (1956), Vol. 17.
14) G. H. Parker and C. A. Mead, *Phys. Rev.*, **184**, 780 (1969).
15) If carrier in semiconductor is produced by the shallow donor level, donor is completely ionized at room temperature. Under the condition, the donor density N_D is identical with the electron density n in semiconductor bulk. Then, the tunneling probability in Eq. 8 was expressed with the electron density n instead of the donor density N_D.
16) R. R. Dogonadze, A. M. Kuznetsov, and V. G. Levich, *Electrochimica. Acta*, **13**, 1025 (1968).
17) E. C. Dutoit, R. L. van Meihaeghe, and F. Cardon, *Ber. Bunsenges. Phys. Chem.*, **79**, 1206 (1975).
18) J. M. Bolts and M. S. Wrighton, *J. Phys. Chem.*, **80**, 2641 (1976).
19) R. Memming and R. Möller, *Ber. Bunsenges. Phys. Chem.*, **76**, 475 (1972).
20) J. A. Mauley and R. C. Dockerty, *Phys. Rev. A*, **140**, 304 (1965).
21) A. G. Chynoweth, W. L. Feldmann, G. A. Lee, R. A. Rogan, and G. L. Person, *Phys. Rev.*, **118**, 425 (1960).
22) T. P. Brody, *J. Appl. Phys.*, **33**, 100 (1962).
23) R. Greef and H. Aulich, *J. Electroanal. Chem.*, **18**, 295 (1968).
24) R. A. Marcus, *Ann. Rev. Phys. Chem.*, **15**, 155 (1964).
25) J. O'M. Bockris and S. U. M. Khan, "Quantum Electrochemistry," Plenum Press, New York (1979).
26) J. W. Schultze, *Z. Phys. Chem.*, **73**, 29 (1970); P. Kohl and J. W. Schultze, *Ber. Bunsenges. Phys. Chem.*, **77**, 953 (1973).
27) H. Taube, *Adv. Chem. Ser.*, **162**, 127 (1977).
28) V. Balzani, F. Scandola, G. Orlandi, N. Sabbatini, and M. T. Indelli, *J. Am. Chem. Soc.*, **103**, 3370 (1981).
29) I. Nagasawa and T. Shimanouchi, *Spectrochim. Acta*, **20**, 429 (1964).
30) K. E. Heusler and Kyung Suk Yun, *Electrochim. Acta*, **22**, 977 (1977).